Accurate evaluation of 3D stress fields in adhesive bonded joints via higher-order FE models

Accurate evaluation of 3D stress fields in adhesive bonded joints via higher-order FE models

A.G. de Miguel*[1], A. Pagani†[1], L. Rizzo‡[1], A. Catapano§[2], and E. Panettieri¶[2]

[1]MUL[2] Group, Department of Mechanical and Aerospace Engineering, Politecnico di Torino, Turin, Italy

[2]Bordeaux INP, Arts et Métiers ParisTech, Université de Bordeaux, Laboratoire I2M CNRS UMR 5295, Talence, France

Abstract

The accurate representation of the 3D stress fields at the bonded areas of adhesive joints is essential for their design and strength evaluation. In the present study, higher-order beam models developed in the framework of the Carrera Unified Formulation (CUF) are employed to reduce the complexity and computational cost of numerical simulations on adhesive joints. The different components of the adhesive joint, i.e. adherends and adhesive, are modeled as beams with independent kinematics based on the Hierarchical Legendre Expansion (HLE). HLE models make use of a hierarchical polynomial expansion over the cross-section of the beam, thus allowing for the control of the accuracy of the stress solutions via the polynomial expansion. Recalling the Finite Element (FE) method, the beam axis is discretised by means of 1D elements. In this manner, generic geometries of the adhesive bonded joints can be studied. The proposed model is assessed through comparison against numerical and analytical references from the literature for single lap and double lap joints. Finally, a detailed 3D analysis is performed on the single lap joint problem, showing that the stress gradients along the adhesive are correctly and efficiently described if the proposed methodology is employed.

Keywords: Adhesive joints, Single lap joint, Refined beam theories, Finite element method, Carrera Unified Formulation, Hierarchical Legendre Expansions.

*Ph.D. Student, alberto.garcia@polito.it

†Assistant Professor, alfonso.pagani@polito.it

‡Graduated research assistant, luca.rizzo@studenti.polito.it

§Associate Professor, anita.catapano@bordeaux-inp.fr

¶Ph.D., enrico.panettieri@u-bordeaux.fr

1 Introduction

Adhesive bonded joints represent an increasingly accepted alternative to mechanical joints in engineering applications, providing many advantages over conventional mechanical fasteners. Continuous junction techniques (welding and bonding) are more convenient than riveting and bolting to match heterogeneous materials, especially for composite materials made of several layers. Indeed, mechanical joints require a preliminary drilling and, therefore, inherent damage to the adherends (for instance interruption of the fibers in composites), causing local stress concentrations. On the other hand, bonded joints are characterized by their good stiffness, lightweight, and good static and fatigue strength. This is due especially to the absence of significant notch effects on the components to be joined together [1]. However, the presence of stress singularities and the elevated stress gradients near the free edges of the bonded region can cause premature debonding phenomena which drastically limit their use [2]. A comparison between the performance of mechanical and adhesive bonding teccniques was carried out by Marannano [3].

In order to study in detail the stress fields that arise in adhesive bonded joints, in the last decades many analytical and numerical models have been developed to support the experimental tests. In particular, most of the analytical theories available in the literature are based on plane strain assumptions. Early studies on bonded joints were carried out by Volkersen [4] and Bikerman [5]. The former studied the adhesive shear stress distribution along the bond line introducing the concept of differential shear and assuming that the behaviour of both the adherend and adhesive materials as linear. The latter one dealt with hybrid adhesives assuming also that both the flexible and stiff substrates behave as perfectly elastic materials. Goland and Reissner [6] explored the effects of the adherend bending leading on the peel stress generated in the adhesive layer. Ojalvo and Eidinoff's model [7] neglected the shear stresses in the bonding material when compared with those in the adherends and, therefore, the adherends deform as thin plates. Under these assumptions, the variation of shear stress through the adhesive thickness was predicted. Hart-Smith [8], unlike [4] and [6], considered adhesive plasticity by combinig elastic peel stress with plastic shear stresses, and modeled the joint using a bi-linear elasto-plastic approximation. Pickett and Hollaway [9] and Lubkin and Reissner [10] analyzed the stresses in tubular lap joints under a tensile axial load. The models they proposed assumed that the adhesive can be approximated to an infinite number of tensile and shear springs and that the transverse stresses in the adherends can be neglected.

Due to its versatility, the Finite Element (FE) method and similar numerical techniques have been widely applied to determine the complex mechanical response of adhesive joints. Adams and Peppiatt [11] studied the tubular lap joint presented in [9] under axial and torsional loads using different meshes of isoparametric eight-node elements. Vable and Maddi [12] employed the Boundary Element Method (BEM) to evaluate the stress fields in single lap joints. Rodriguez et al. [13] compared the performance of FEM software tools against analytical models from the literature for the single lap joint. Three-dimensional FE analysis were perfomred by Kaya and Tekelioglu [14], who used hexahedral elements considering both aluminum and steel as

adherends. Afshar et. al. [15] studied the intensity of the in-plane and out-of-plane stress distributions along the plate width direction, and the effects of adhesive thickness and Poisson's ratio.

The aforementioned works based on the FE method are based on standard 2D and 3D models. The present work introduces the use of higher-order beam theories to evaluate the stress fields in the bonded zone of adhesive joints. To achieve this purpose, the Carrera Unified Formulation (CUF) [16] is recalled to generate layerwise (LW) theories which account for the different components of the joint, i.e. adherends and adhesive. A previously introduced beam theory, the so-called Hierarchical Legendre Expansion (HLE) [17], is employed to obtain accurate stress fields over the adhesive layer.

The structure of the paper is the following one: a description of refined models based on the CUF and the HLE theory is presented in Section (2), the implementation of a corresponding beam element is provided in Section (3), the numerical assessment of the model is included in Section (4), together with a detailed 3D analysis of the adhesive layer of a typical single lap joint. Finally, the conclusion and future prospects are drawn in Section (5).

2 Refined beam models based on CUF

The Carrera Unified Formulation (CUF) was developed by Carrera [16] and his collaborators in the 1990s as a hierarchical formulation to generate refined theories of structures. The CUF is based on the idea that non-classical effects (e.g. shear effects, warping, planar deformations, bending and torsional behaviour) can be studied via models characterized by refined kinematics. In the CUF framework, the displacement fields of a beam model can be described by series of generic functions F_τ:

$$\mathbf{u}(x, y, z) = F_\tau(x, z)\mathbf{u}_\tau(y), \quad \tau = 1, \ldots, \mathrm{M} \tag{1}$$

where F_τ are the functions approximating the generalized variable of displacements u over the cross-section, u_τ is the displacement vector and M is the number of the terms for the series; the choice of F_τ and M is arbitrary, thus different base functions of any order can be chosen to assume the deformation of the cross-section of the beam. In Eq. 1, (x, y, z) represents a Cartesian coordinate system, where y lays along the beam axis and (x, z) are the coordinates of the cross-section.

In the last years, several theories of structure have been implemented in the proposed framework. A well-known example is the so-called Taylor Expansion (TE), which is based on a Taylor-class polynomial expansions of the displacements field over the cross-section of the structure. In TE models, the order N of the expansion is arbitrary and is set as an input of the analysis. For example, the second-order model $N = 2$ has the following kinematic field, see

[18, 19]:

$$\begin{aligned} u_x = &\ u_{x1} + xu_{x2} + zu_{x3} + x^2u_{x4} + xzu_{x5} + z^2u_{x6}, \\ u_y = &\ u_{y1} + xu_{y2} + zu_{y3} + x^2u_{y4} + xzu_{y5} + z^2u_{y6}, \\ u_z = &\ u_{z1} + xu_{z2} + zu_{z3} + x^2u_{z4} + xzu_{z5} + z^2u_{z6} \end{aligned} \tag{2}$$

Classical beam theories are obtainable as particular cases of Taylor expansions for $N = 1$. However, the use of TE has some intrinsic limitations for the accurate study of complex structures: first of all, the higher-order variables have only a mathematical meaning and, therefore, they are not directly related to a physical response. This drawback can be a limit for the evaluation of localized effects, such as the stress fields in adhesive joints.

An improvement of the beam kinematics towards the accurate 3D analysis of beam-like structures was introduced by Carrera and Petrolo [20], who used the Lagrange Expansion (LE). LE exploits Lagrange polynomials, whose advantage is twofold: first these interpolating polynomials allows to have only displacements variables and, second, one can opportunely enrich the most important zones of the structure with many sub-domains to provide a better description of localized phenomena. Moreover, the use of mathematical domains over the cross-section makes LE a suitable model for the development of advanced layerwise models [21]. The Lagrange functions used to generate nine-node quadrilateral expansions (L9) are reported in the following:

$$\begin{aligned} F_\tau = &\ \tfrac{1}{4}(r^2 + rr_\tau)(s^2 + ss_\tau), \qquad \tau = 1, 3, 5, 7 \\ F_\tau = &\ \tfrac{1}{2}s_\tau^2(s^2 - ss_\tau)(1 - r^2) + \tfrac{1}{2}r_\tau^2(r^2 - rr_\tau)(1 - s^2), \qquad \tau = 2, 4, 6, 8 \\ F_\tau = &\ (1 - r^2)(1 - s^2) \qquad \tau = 9 \end{aligned} \tag{3}$$

in which r and s can vary between -1 and 1 and r_τ and s_τ are the coordinates of the cross-sectional reference nodes, see Ref. [21]. The displacement field of a L9 element can be written as:

$$\begin{aligned} u_x = &\ F_1u_{x1} + F_2u_{x2} + F_3u_{x3} + F_4u_{x4} + F_5u_{x5} + F_6u_{x6} + F_7u_{x7} + F_8u_{x8} + F_9u_{x9}, \\ u_y = &\ F_1u_{y1} + F_2u_{y2} + F_3u_{y3} + F_4u_{y4} + F_5u_{y5} + F_6u_{y6} + F_7u_{y7} + F_8u_{y8} + F_9u_{y9}, \\ u_z = &\ F_1u_{z1} + F_2u_{z2} + F_3u_{z3} + F_4u_{z4} + F_5u_{z5} + F_6u_{z6} + F_7u_{z7} + F_8u_{z8} + F_9u_{z9} \end{aligned} \tag{4}$$

where $u_{x1}, \ldots, u_{z9}$ are the displacement variables over the expansion domain.

2.1 The hierarchical Legendre expansion

A further development for the accurate modeling of beam structures was represented by the introduction of the HLE. This theory was first implemented by Carrera et al. [17] and includes some the advantages of TE and LE models. HLE models express the 3D displacements field as LE of the generalized displacements over the section. Similarly to TE, the expansion order is increased in a hierarchical manner in the case of HLE. Furthermore, their kinematics can also be enriched locally over the physical surface of the cross-section as per LE. The mathematical

description of HLE, based on the work of Szabó and Babuška [22], is drawn here below.

The 1D Legendre polynomials can be defined as:

$$\begin{aligned} L_0 &= 1, \\ L_1 &= x, \\ L_k &= \tfrac{2k-1}{k} x L_{k-1}(x) - \tfrac{k-1}{k} L_{k-2} \quad k = 2,3, \ldots \end{aligned} \tag{5}$$

These polynomials form an orthonormal basis and their roots are identical with integration points of Gauss quadrature rules. A set of 1D functions deriving from these polynomials is:

$$\begin{aligned} L_1(r) &= \tfrac{1}{2}(1-r), \\ L_2(r) &= \tfrac{1}{2}(1+r), \\ L_i(r) &= \phi_{i-1}(r) \quad i = 3,4, \ldots, \text{p+1} \end{aligned} \tag{6}$$

in which r is the local coordinate in the 1D domain [-1,1] and the function $\phi_j(r)$ is defined as:

$$\phi_j(r) = \sqrt{\frac{2j-1}{j}} \int_{-1}^{r} L_{j-1}(x)dx, \quad i = 2,\ 3,\ 4,\ \ldots \tag{7}$$

The first two equations of Eq. (6) represent the nodal modes whereas the last one contains all the internal modes along the beam axis between the two extremities. Based on this set of 1D functions, a 2D hierarchical approximation for the cross-sectional assumptions is generated, consisting of vertex, side and internal expansions. The vertex expansions are written as:

$$F_\tau = \frac{1}{4}(1 - r_\tau r)(1 - s_\tau s), \quad \tau = 1,\ 2,\ 3,\ 4 \tag{8}$$

in which r and s vary in the range [-1,1] above the domain while r_τ and s_τ are the vertex coordinates in the natural plane.

The side expansions exist only for $p \geq 2$ (p being the polynomial degree) and they are defined as:

$$\begin{aligned} F_\tau(r,s) &= \tfrac{1}{2}(1-s)\phi_p(r), \quad \tau = 5,\ 9,\ 13,\ 18,\ \ldots \\ F_\tau(r,s) &= \tfrac{1}{2}(1+r)\phi_p(s), \quad \tau = 6,\ 10,\ 14,\ 19,\ \ldots \\ F_\tau(r,s) &= \tfrac{1}{2}(1+s)\phi_p(r), \quad \tau = 7,\ 11,\ 15,\ 20,\ \ldots \\ F_\tau(r,s) &= \tfrac{1}{2}(1-r)\phi_p(s) \quad \tau = 8,\ 12,\ 16,\ 21,\ \ldots \end{aligned} \tag{9}$$

The internal expansions are defined for $p \geq 4$ as a product of the 1D internal modes of Eq. (6). For the sake of clarity, the expressions of the corresponding internal expansions of sixth order are included:

$$\begin{aligned} F_{28}(r,s) &= \phi_4(r)\phi_2(s), \\ F_{29}(r,s) &= \phi_3(r)\phi_3(s), \\ F_{30}(r,s) &= \phi_2(r)\phi_4(s) \end{aligned} \tag{10}$$

Fig. 1 shows the complete set of polynomial expansions used to defined the beam kinematics from the first to the seventh order.

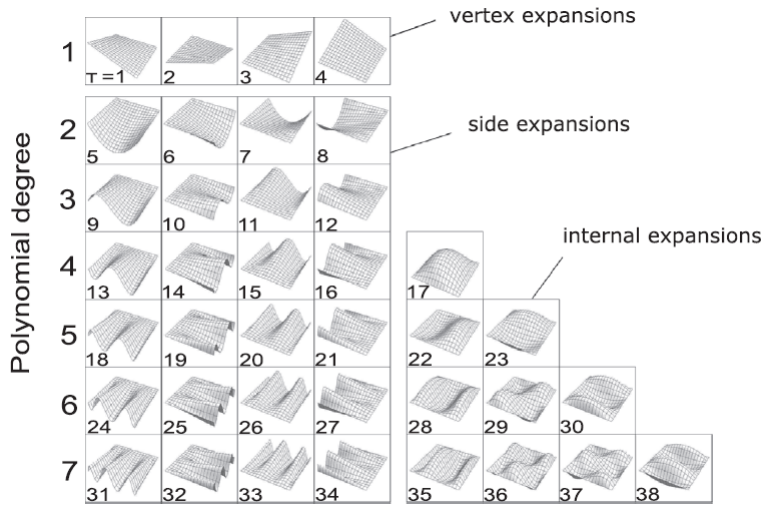

Figure 1: Hierarchical LE F_τ used for HLE models from linear to 7^{th} expansion order [17].

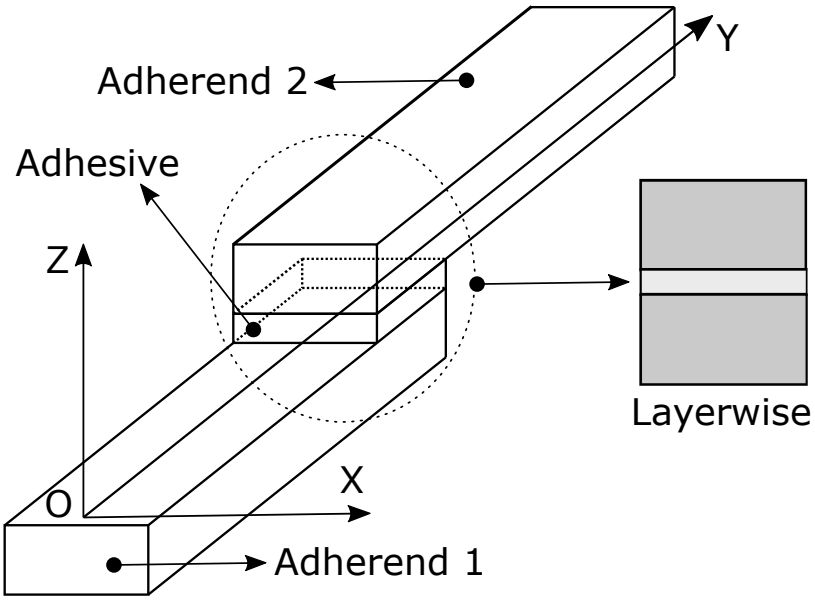

Figure 2: Layerwise approach in adhesive joints.

2.2 Layerwise approach for adhesive joints

For HLE modeling and layerwise approach, each layer of the bonded area is modeled assuming an independent kinematics. The continuity of the displacements is defined at the interface of the plies in the cross-section domain. In LW the number of degrees of freedom depends directly on the number of layers, thus Eq. (1) becomes:

$$\mathbf{u}(x, y, z) = F_\tau(x, z)\mathbf{u}^k_\tau(y), \quad \tau = 1, \ldots, \mathrm{M} \tag{11}$$

k being the index referring to each layer. If we assume that adhesive and adherend are perfectly bonded, see Fig. 2, the compatibility conditions are introduced in the model as:

$$\begin{array}{rcl} \mathbf{u}_{bottom}^{adhesive} & = & \mathbf{u}_{top}^{adherend1}, \\ \mathbf{u}_{top}^{adhesive} & = & \mathbf{u}_{bottom}^{adherend2} \end{array} \tag{12}$$

which is imposed by assembling the vertex and side expansions at the interfaces *top* and *bottom*.

The proposed LW formulation allows for enhancing the kinematic field of the adhesive by means of the polynomial order of the HLE model. In the proposed model, as the geometrical and mechanical parameters are defined, the convergence of the stress solutions is sough varying the HLE order in an automatic and hierarchical manner.

3 Finite Element Formulation

In the present work, the FE method is used to derive the governing equations of the elasticity problem. The beam axis is discretized using standard beam elements. Thus, Eq. (1) becomes:

$$\mathbf{u}(x, y, z) = F_\tau(x, z) N_i(y) \mathbf{u}_{\tau i}^k \tag{13}$$

where N_i stands for the shape functions and $\boldsymbol{u_{\tau i}}$ are the unknown nodal vector. Considering y the principal axis of the beam, Eq. (13) can be rewritten as:

$$\mathbf{u}_\tau(y) = N_i(y) \mathbf{u}_{\tau i}, \quad \text{i} = 1, 2, \ldots, \text{n} \tag{14}$$

where n is the number of shape functions per element and the unknown nodal vector can finally be expressed as the following one:

$$\mathbf{u}_{\tau i} = \left\{ u_{u_{x_{\tau i}}}, u_{u_{y_{\tau i}}}, u_{u_{z_{\tau i}}} \right\}^T \tag{15}$$

Now, according to the matrix representation of the classical elasticity theory, stresses $\boldsymbol{\sigma}$ and strains $\boldsymbol{\varepsilon}$ can be written in vectorial form as follows:

$$\boldsymbol{\sigma}^T = \{\sigma_{yy},\ \sigma_{xx},\ \sigma_{zz},\ \sigma_{xz},\ \sigma_{yz},\ \sigma_{xy}\} \tag{16}$$

$$\boldsymbol{\varepsilon}^T = \{\varepsilon_{yy},\ \varepsilon_{xx},\ \varepsilon_{zz},\ \varepsilon_{xz},\ \varepsilon_{yz},\ \varepsilon_{xy},\} \tag{17}$$

The geometrical relations between strains and displacements can be defined as:

$$\boldsymbol{\varepsilon} = \mathbf{D}\mathbf{u} \tag{18}$$

where $\mathbf{D}$ is the following differential operator:

$$\mathbf{D} = \begin{bmatrix} 0 & \frac{\partial}{\partial y} & 0 \\ \frac{\partial}{\partial x} & 0 & 0 \\ 0 & 0 & \frac{\partial}{\partial z} \\ \frac{\partial}{\partial z} & 0 & \frac{\partial}{\partial x} \\ 0 & \frac{\partial}{\partial z} & \frac{\partial}{\partial y} \\ \frac{\partial}{\partial y} & \frac{\partial}{\partial x} & 0 \end{bmatrix} \tag{19}$$

The physical relation between stresses and strains is defined by the Hooke's law:

$$\boldsymbol{\sigma} = \mathbf{C}\ \boldsymbol{\varepsilon} \tag{20}$$

where $\mathbf{C}$ is the stiffness matrix.

3.1 Stiffness Matrix

According to the principle of virtual displacements, in CUF the work made by internal forces can be written as:

$$\delta L_{int} = \int_V (\delta \boldsymbol{\varepsilon}^T \boldsymbol{\sigma}) dV = \delta L_{ext} \tag{21}$$

where V is the volume domain of the body, δL_{int} is the internal work (strain energy), δL_{ext} is the external work and δ stands for the virtual variation. Substituting the constitutive equations for the materials and the geometrical relations along with CUF, the internal work can be rewritten in a simple way:

$$\delta L_{int} = \delta \mathbf{q}_{\tau i}^T \boldsymbol{K}^{ij\tau s} \mathbf{q}_{sj} \tag{22}$$

where $\mathbf{K}^{ij\tau s}$ is:

$$\boldsymbol{K}^{ij\tau s} = \int_l \int_\Omega \boldsymbol{D}^T (N_i F_\tau \boldsymbol{I}) \boldsymbol{C} \boldsymbol{D} (N_j F_s \boldsymbol{I}) d\Omega ds \tag{23}$$

The array $\mathbf{K}^{ij\tau s}$ is the 3×3 fundamental nucleus of the stiffness matrix and it does not depend on the expansion order of the theory or on the polynomial expansion F_τ. The components of the fundamental nucleus for isotropic structures are expressed in the following:

$$\begin{aligned} K_{\alpha\alpha}^{\tau sij} &= (\lambda + 2G) \int_l N_i\, N_j\, \mathrm{d}y \int_\Omega F_{\tau,x} F_{s,x}\, d\Omega + G \int_l N_i\, N_j\, \mathrm{d}y \int_\Omega F_{\tau,z} F_{s,z}\, d\Omega + \\ &\quad + G \int_l N_{i,y}\, N_{j,y}\, \mathrm{d}y \int_\Omega F_\tau F_s\, d\Omega \\ K_{\alpha\beta}^{\tau sij} &= \lambda \int_l N_i\, N_{j,y}\, \mathrm{d}y \int_\Omega F_\tau F_{s,x}\, d\Omega + G \int_l N_{i,y}\, N_j\, \mathrm{d}y \int_\Omega F_{\tau,x} F_s\, d\Omega \end{aligned} \tag{24}$$

where $\alpha, \beta = x, y, z$. It is intended, in fact, that all the nine components of the stiffness nucleus can be obtained by permutations from Eq. (24), depending only on the material coefficients, λ

and G which are the Lamé's parameters expressed as $G = \frac{E}{2(1+\nu)}$ and $\lambda = \frac{\nu E}{(1+\nu)(1-2\nu)}$.

Finally, the work of the external forces δL_{ext} can be expressed as:

$$\delta L_{ext} = \int_V (\delta \mathbf{u}^T \mathbf{F})\, dV = \delta \mathbf{q}_{\tau i}^T \int_V (N_i(y) F_\tau(x,z) \tilde{\mathbf{F}})\, dV = \delta \mathbf{q}_{\tau i}^T \mathbf{F}^{\tau i} \tag{25}$$

where $\tilde{\mathbf{F}}$ is the generic load and $\mathbf{F}^{\tau i}$ is the vector of the nodal forces. Finally, the following linear algebraic system has to be solved:

$$\tilde{\mathbf{K}} \mathbf{u} = \tilde{\mathbf{F}} \tag{26}$$

in which $\tilde{\mathbf{K}}$ is the global stiffness, $\mathbf{u}$ is the vector of the unknowns and $\tilde{\mathbf{F}}$ is the force vector, respectively.

4 Numerical results

This section presents the results obtained from the static analysis of bonded joints through the use of HLE models. The first analysis carried out concerns a single lap joint, then the second part is related to the study of a double lap joint with a combination of stiff and flexible adhesives along the bondline. Both models show a comparison between HLE and numerical or analytical results taken from literature.

4.1 Single Lap Joint

The geometry and the dimensions of the single lap joint are chosen in accordance with the ASTM D1002 standard [23] (Fig. 3). An isotropic material is employed for both the adherends and the adhesive with the following properties: $E_{Adherends} = 73100\,\text{MPa}$, $E_{Adhesive} = 1120\,\text{MPa}$, $\nu_{Adherends} = 0.34$, $\nu_{Adhesive} = 0.33$. The single lap joint is clamped at $y = 0$ and loaded at $y = L$ with an equivalent force of 1000 N oriented towards the y-direction (Fig. 2), defining a model equivalent to the one studied by Rodriguez et. al. [13].

The stresses are evaluated for HLE models including polynomial orders up to the 8^{th} (see Table 1). 20 four-node B4 elements are employed with graded refinements in the bonded area towards the edges. The stresses are evaluated in the middle plane of the adhesive. The distribution of normal and shear stresses along the overlap region are plotted in Figs. 4 and 5. The adhesive is divided into 2 hierarchical domains along the z-axis and plain strain assumptions are adopted on the x-direction.

Respectively, the peel (or normal) stress corresponds to σ_{zz} and the shear stress to σ_{yz}. For peel stress (Fig. 4) the fast convergence from HLE 2 up to HLE 8 is clear. Although the HLE 1 overestimates the stresses at the edges, a polynomial order 2 and higher tend to show a gradient change of σ_{zz}. Moreover, at the free edges of the adhesive the stress σ_{yz} must be negligible to satisfy the equilibrium conditions. Accordingly, the shear stress (Fig. 5) shows a particular shape in the free edges, only detected by the HLE orders from 2^{nd} to 7^{th}: it varies, in

Model	σ_{zz} [MPa]	σ_{yz} [MPa]	DOFs
HLE 1	16.862	6.609	2859
HLE 2	11.635	7.958	2859
HLE 3	10.752	7.252	4428
HLE 4	10.791	7.378	6459
HLE 5	10.736	7.234	8952
HLE 6	10.804	7.258	11907
HLE 7	10.812	7.249	15324

Table 1: Maximum stress values of peel and shear stresses and number of degrees of freedom of each model (DOFs).

very few millimetres, from a low value to the maximum one (7.248 MPa), therefore this region is characterized by the highest stress gradients of the adhesive. In order to correctly predict such mechanical behavior higher polynomials orders are needed (Table 1).

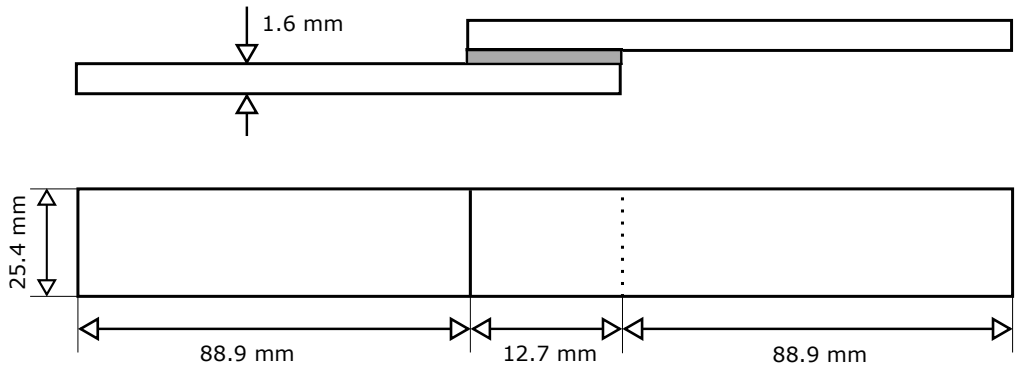

Figure 3: Single lap joint: geometrical dimensions.

Finally, a comparison with results taken from literature is shown in Figs. 6 and 7. From the references, the numerical model [13] was the only one able to approximate the zero shear stress at the free end of the adhesive layer. HLE models assure a good correspondence with both analytical and numerical solutions.

4.2 Hybrid-adhesive double lap joint

In order to reduce peel and shear stresses, a combination of stiff and flexible adhesives along the bondline can be used, as reported by Pires et al. [24]. Pires' results indicate that joints' strength can be optimized by appropriate geometrical and material selection. For example, joints with bi-adhesive bondlines are more resistant than those with single adhesives in the bondline. The double lap joint studied derives from Ozer & Oz's work [25] (the case analysed here is that of $l_f/l_s = 0.7$): Aluminum alloy 7075 was used for inner and outer adherends, Hysol EA9313 and Terokal 5045 were used as stiff and flexible epoxy adhesives, respectively.

The geometrical dimensions of the double lap joint are described in Fig. 8: width along x-axis = 25 mm, $T_A = 1.75$ mm, $T_a = 0.25$ mm, $l_f = 3.6456$ mm, $l_s = 5.208$ mm, $L_a = 87.5$ mm. The material properties of both adherends and adhesives are presented in Table 2, where

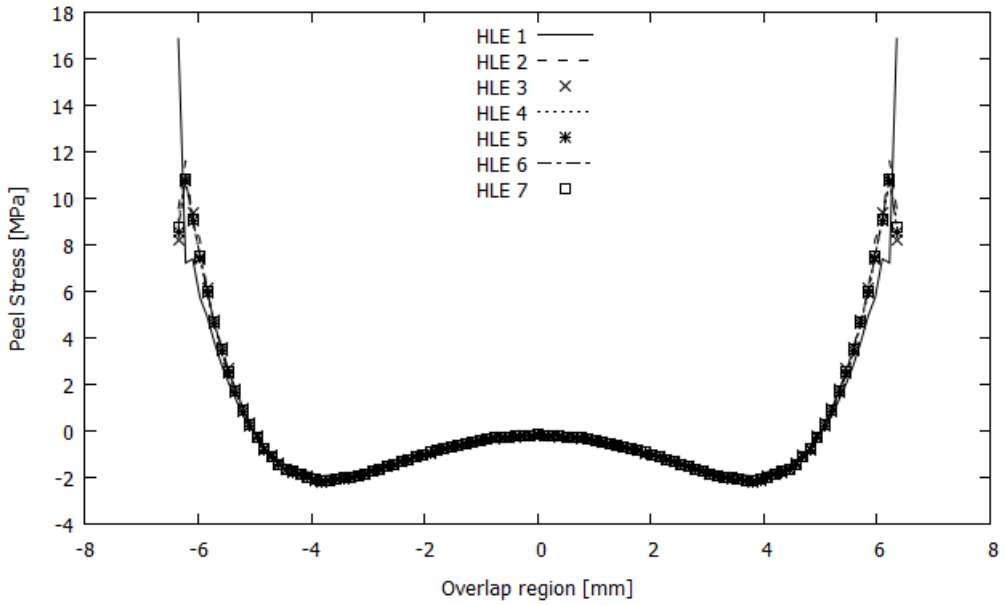

Figure 4: Single lap joint: peel stress convergence analysis.

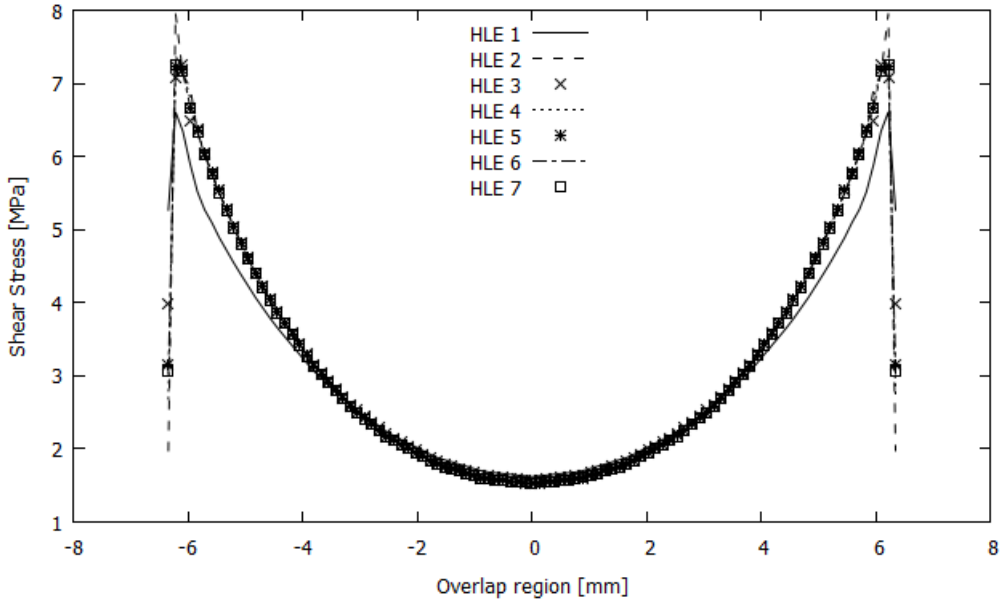

Figure 5: Single lap joint: shear stress convergence analysis.

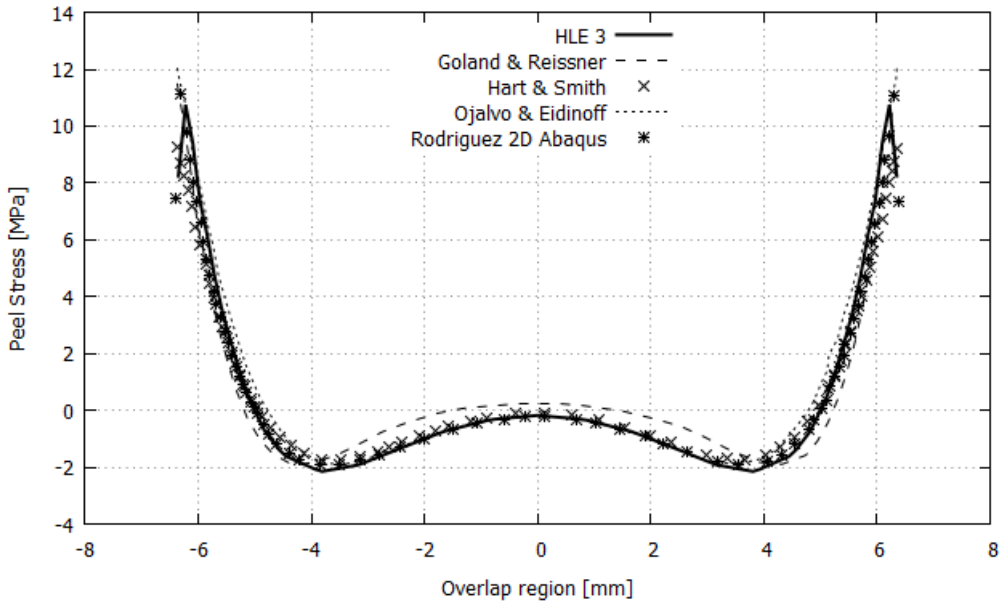

Figure 6: Comparison of peel stress distribution.

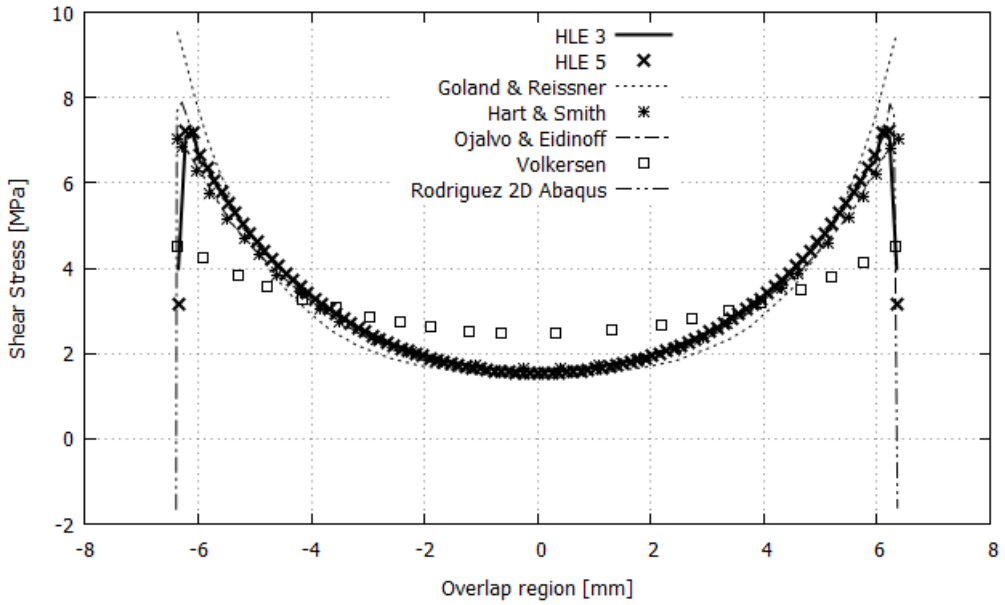

Figure 7: Comparison of shear stress distribution.

E_{Al}, E_{FA}, E_{SA} stand for the Young's Modulus of the adherends, the flexible adhesive and the stiff adhesive, respectively; and ν_{Al}, ν_{FA}, ν_{SA} stand for the Poisson's ratio of the same materials.

Property	Value
E_{Al}	71.7 GPa
E_{FA}	0.437 GPa
E_{SA}	2.274 GPa
ν_{Al}	0.33
ν_{FA}	0.38
ν_{SA}	0.36

Table 2: Material properties of the double lap joint (see Fig. 8).

The joint is loaded on the left side of the inner adherend (i.e. at y=-87.5 mm) with four point forces applied at the corners of the tip cross-section. Each force is equal to 250 N and they are oriented towards the y-direction. HLE stress solutions of orders 6 and 7 are shown in Table 3 for convergence purposes, where σ_{zz} refers to the peel (or normal) stress and σ_{xz} refers to the shear stress. All stresses are normalised by the average value of σ_{yz}.

The same longitudinal mesh of the previous case is used, but in this case 5 cross-sections are created in order to account for the variation of the adhesives properties in the longitudinal direction (see Fig. 9). The stresses are evaluated at the middle plane of the adhesive. The distribution of normal and shear stresses along the overlap region are plotted in Fig. 10 and 11 and compared with the results from [25]. It is possible to observe that HLE beam are able to represent highly complex stress fields, showing small errors in comparison to the analytical results provided by Ozer & Oz [25], predicting the peak values at the adhesive interfaces.

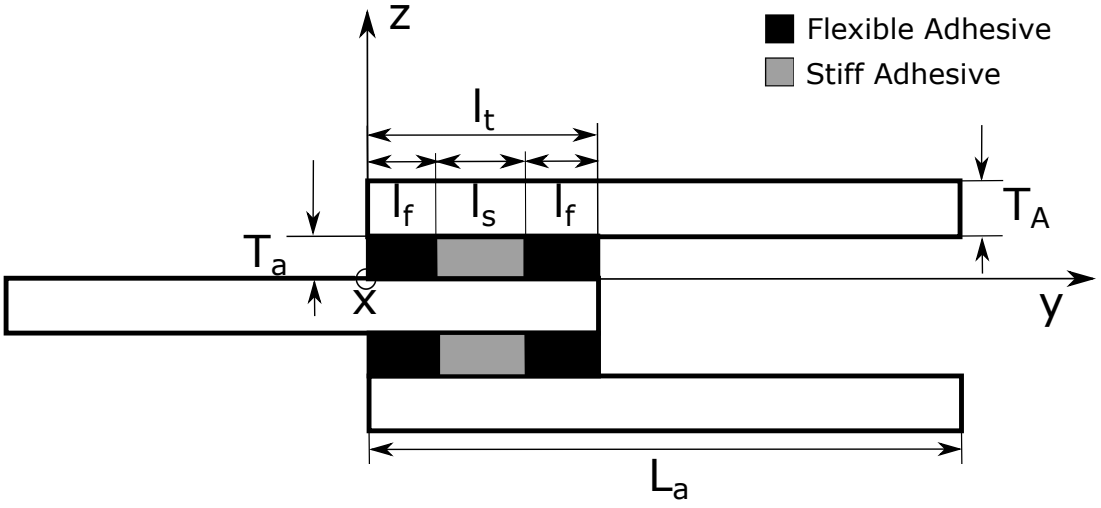

Figure 8: Double Lap Joint, Ozer & Oz [25].

4.3 3D analysis of the single lap joint

Plain strain models provide useful knowledge about the stress distributions in adhesive joints and the evaluation of the failure indexes. However, the assumption of infinite width in the x

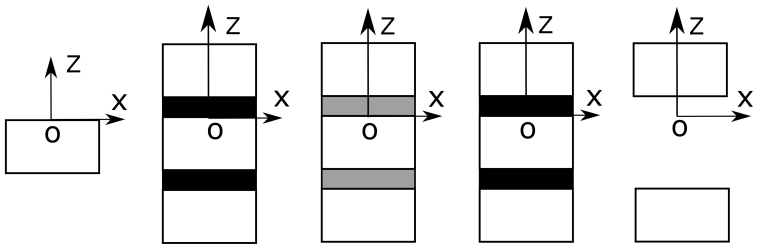

Figure 9: Hybrid-adhesive double lap joint cross-section HLE discretization: the three central figures correspond to the LW sections of the different adhesives.

Model	σ_{zz}	σ_{yz}	DOFs
HLE 6	0.6598	1.3741	7722
HLE 7	0.6682	1.3602	9870
Ozer & Oz	0.7032	1.3333	/

Table 3: Maximum values of Peel and Shear stress at the free edges and degrees of freedom of the models generated.

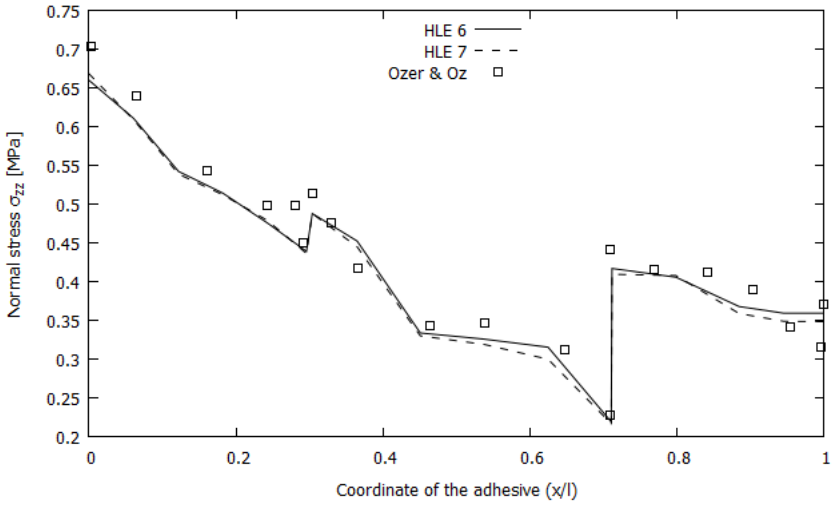

Figure 10: Peel Stress along x-axis.

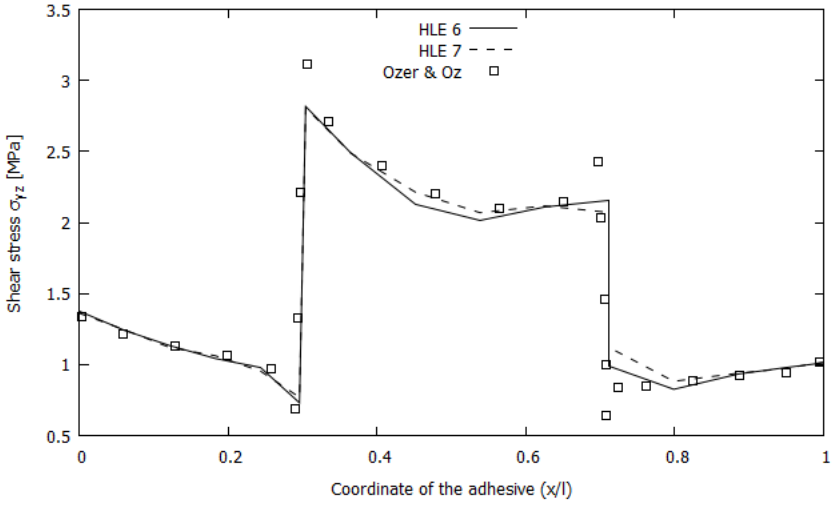

Figure 11: Shear Stress along x-axis.

direction is not always valid and neglects the free-edge effects that arise at the corners of the joints. In order to study the 3D gradients of the stresses in the single lap joint, a distribution of fourth-order HL4 domains is generated over the cross-section surface, as shown in Fig. 12. The symmetry of the structure in the xy-plane is exploited to generate only half of the model. In total, the model accounts for 20,079 degrees of freedom. The geometry and loading is that of Section 4.1. Figure 13 shows a 3D plot of the deformed configuration of the single lap joint under axial loading and the colour map of the longitudinal stress σ_{yy} over the structure, from which it is clear the variation of the solutions along the transverse direction in the bonded area.

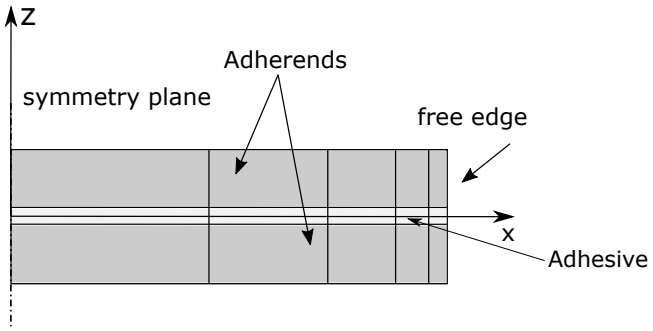

Figure 12: Distribution of HLE domains over the cross-section for the 3D model of the single lap joint.

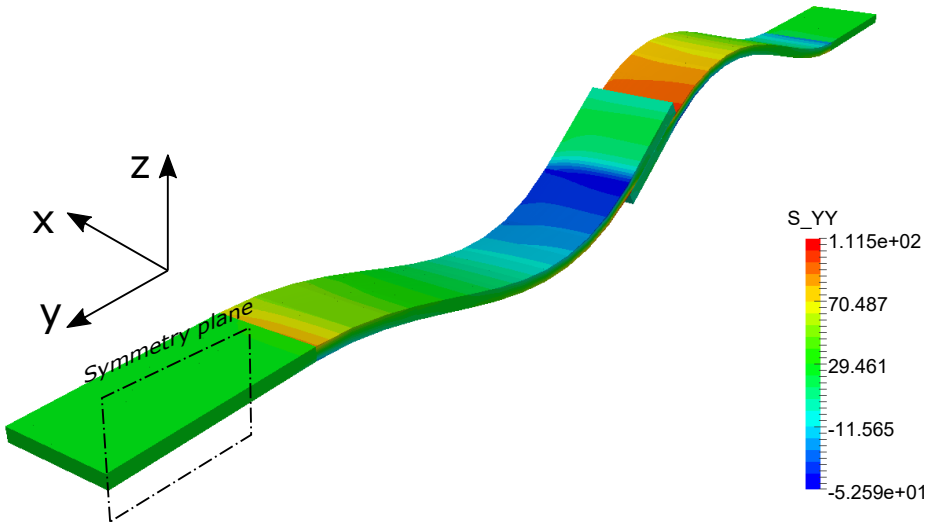

Figure 13: Deformed configuration and longitudinal stresses, σ_{yy}, of the single lap joint specimen under 1000N of axial load.

Taking advantage of the higher-order layerwise capabilities of the HLE models, a detailed study of the stress fields is performed over the adhesive strip volume. Figures 14, 15, 16 and 17 show the distribution of several stress components along the transverse direction, x, at the edge of the joint ($y = 88.9$ mm) for different heights in the adhesive. The legends *bottom* and *top* correspond to the lower and upper, respectively, interfaces with the adherend, whereas *center* stays for the values at the midplane of the adhesive. As it can be seen from the graphs, the

stress solutions vary considerably across the thickness of the adhesive ply, which can influence in a great extent the failure evaluation of the joint. This effect is not accounted in most of the literature dealing with the stress analysis of adhesive joints, which usually reports the stress values at the midplane of the adhesive. Moreover, one can observe the non-neglible variations of all the stress components towards the free corner, in particular at the bottom interface. Moreover, this study suggests that the in-plane shear stresses might also contribute to the adhesive failure at the corners. Finally, Figs. 18, 19 and 20 depicts the 3D plot of σ_{zz}, σ_{yz} and σ_{xz}, respectively, over the adhesive layer.

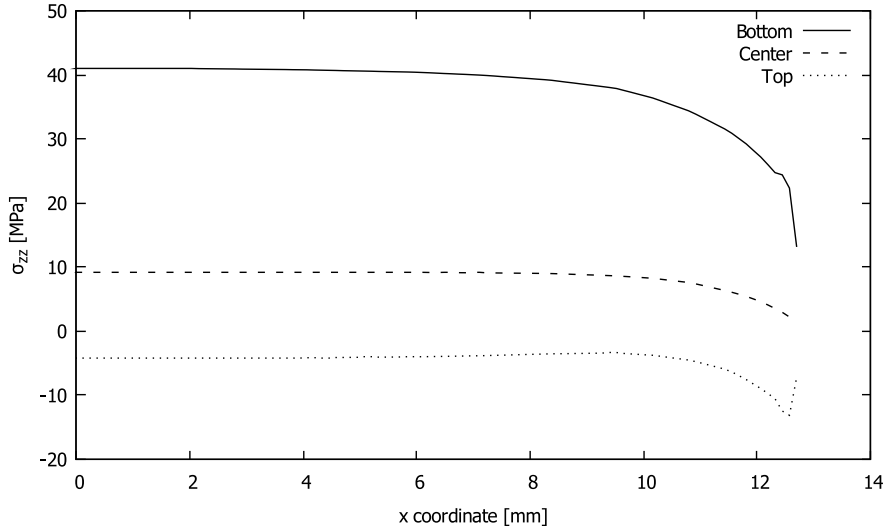

Figure 14: Peel stress, σ_{zz}, along the transverse direction, x, at different points in the adhesive. Model: fourth-order expansion (HLE 4) and 20 cubic beam elements.

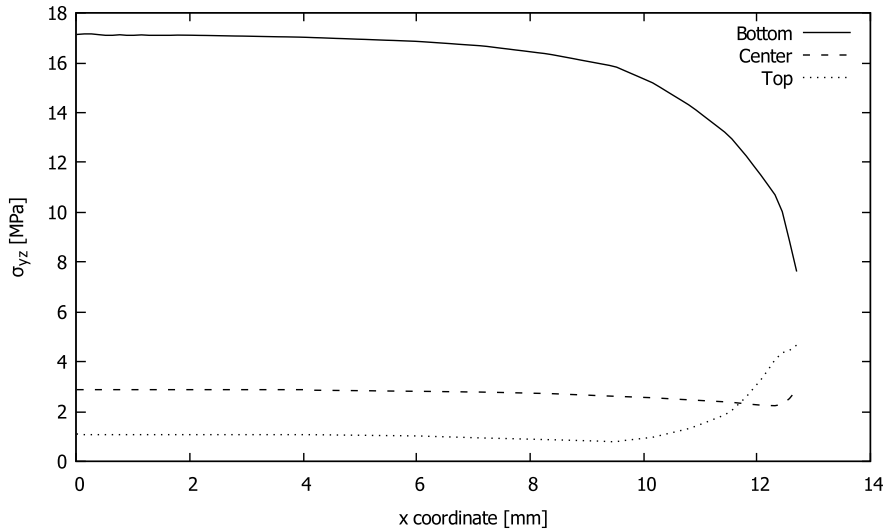

Figure 15: Shear stress, σ_{yz}, along the transverse direction, x, at different points in the adhesive. Model: fourth-order expansion (HLE 4) and 20 cubic beam elements.

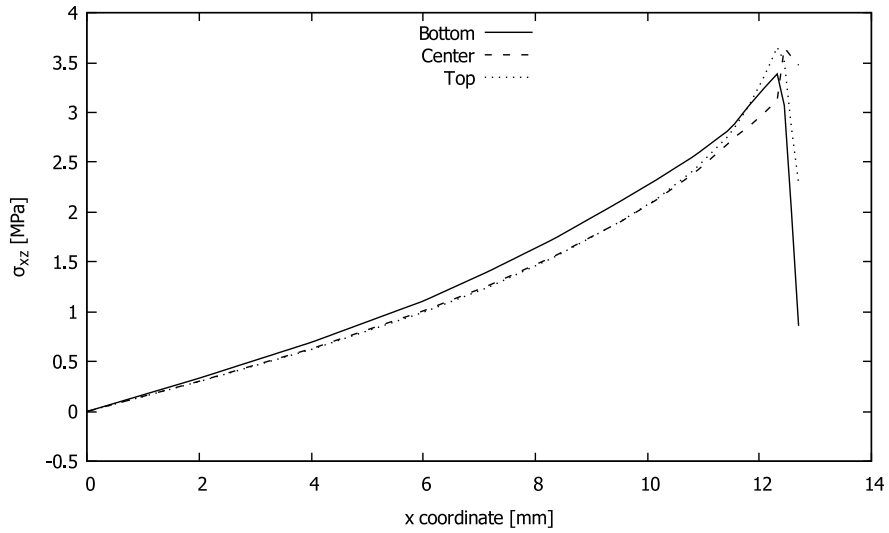

Figure 16: In-plane shear stress, σ_{xz}, along the transverse direction, x, at different points in the adhesive. Model: fourth-order expansion (HLE 4) and 20 cubic beam elements.

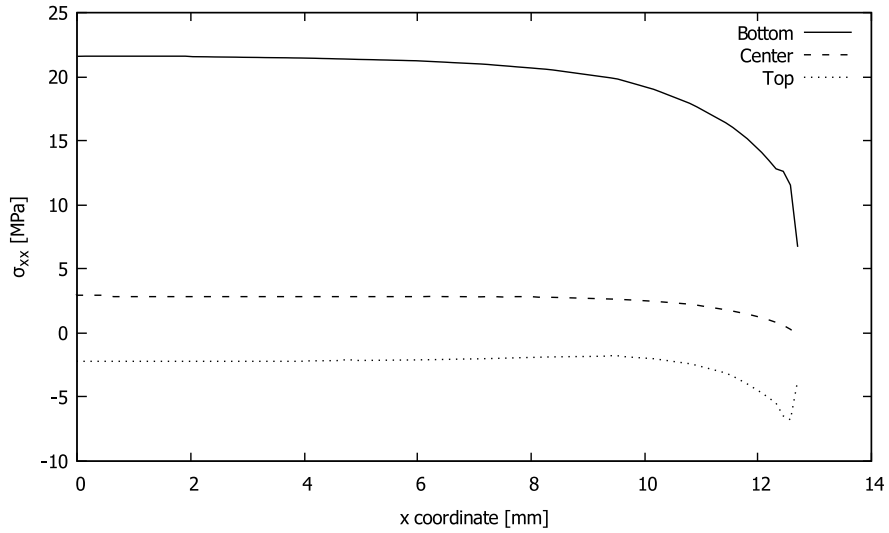

Figure 17: In-plane transverse stress, σ_{xx}, distribution along the transverse direction, x, at different points in the adhesive. Model: fourth-order expansion (HLE 4) and 20 cubic beam elements.

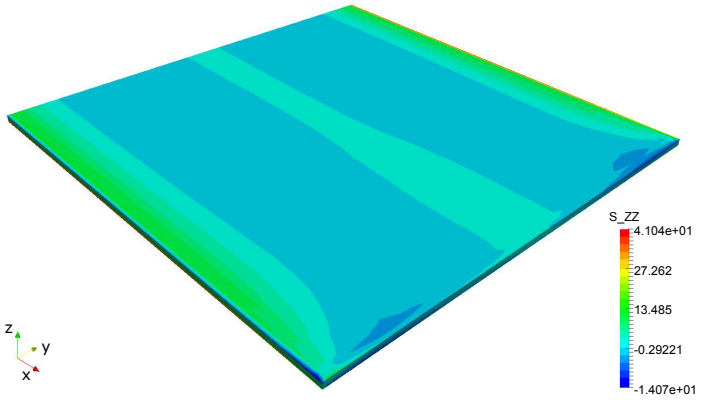

Figure 18: Peel stress, σ_{zz}, over the adhesive layer.

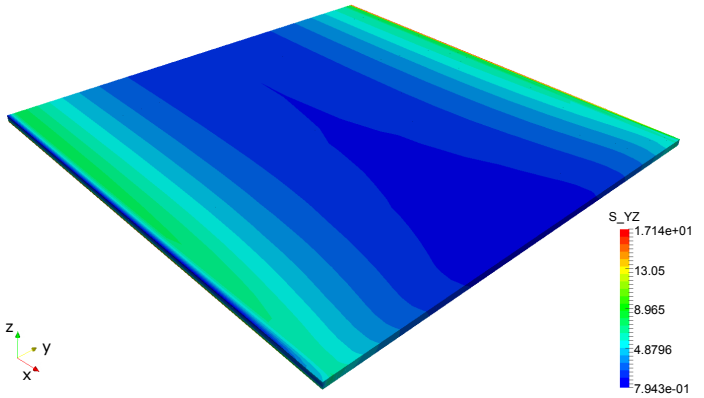

Figure 19: Shear stress, σ_{yz}, over the adhesive layer. Model: fourth-order expansion (HLE 4) and 20 cubic beam elements.

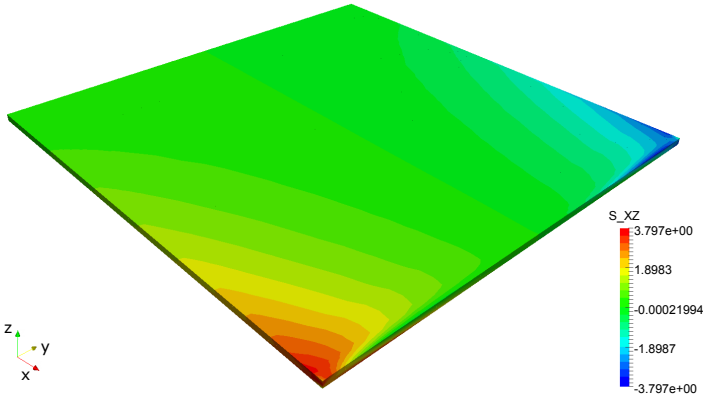

Figure 20: In-plane shear stress, σ_{xz}, over the adhesive layer. Model: fourth-order expansion (HLE 4) and 20 cubic beam elements.

5 Conclusions

This work presents the stress analysis of adhesive bonded joints via higher-order beam models. The Carrera Unified Formulation (CUF) is employed to generate variable kinematic models based on the Hierarchical Legendre Expansion (HLE) and a layerwise (LW) approach at the bonded area. In this manner, each component of the model, i.e. adherends and adhesive, are accounted by means of independent displacement fields represented by Legendre polynomials. Subsequently, it is demonstrated that the accuracy of the stress solutions is increased for polynomials of higher-orders.

Given the efficiency and fidelity of the stress solutions, the proposed method is suitable for parametric studies of adhesive bonded joints. Both analysis of the single lap and double lap joints show a good agreement with the numerical and analytical references from the literature. Finally, new solutions of a detailed 3D analysis of the single lap joint are provided, highlighting the necessity of considering the stress gradients in all directions in the adhesive layer.

References

[1] Anthony Kinloch. Numerical experimental analysis of hybrid double lap aluminum-cfrp joints. *Springer Netherlands*, 1:XII, 442, 1987.

[2] Hart-Smith LJ. Design methodologies for bonded-bolted composite joints. *Flight Dynamics laboratory - Wright Patterson Air Force Baie Aeronautical Laboratories - Ohio*, 48:5–35, 1982.

[3] G. Marannano and B. Zuccarello. Numerical experimental analysis of hybrid double lap aluminum-cfrp joints. *Composites Part B: Engineering*, 71:28 – 39, 2015.

[4] O. Volkersen. Die nietkraftverteilung in zugbeanspruchten nietverbindungen mit konstanten laschenquerschnitten. *Luftfahrtforschung*, 15:41–47, 1938.

[5] J. J. Bikerman. *The Science of Adhesive Joints*. 1968.

[6] E. Reissner M. Goland. The stresses in cemented lap joints. *Journal of Applied Mechanics*, pages A17–A27, 1944.

[7] H. L. Eidinoff I. U. Ojalvo. Bond thickness effects upon stresses in single-lap adhesive joints. *AIAA Journal*, pages 204–211, 1977.

[8] L. J. Hart-Smith. Adhesive-bonded single lap joints. *Journal of Aircraft*, pages 97–104, 1973.

[9] A.K. Pickett and L. Hollaway. The analysis of elastic adhesive stresses in bonded lap joints in frp structures. *Composite Structures*, 3(1):55 – 79, 1985.

[10] J.L.Lubkin and E.Reissner. Stress distribution and design data for adhesive lap joints between circular tubes. *Transaction ASME 78*, pages 1213–1221, 1956.

[11] R Adams and N A. Peppiatt. Stress analysis of adhesive bonded tubular lap joints. 9:1–18, 01 1977.

[12] Madhukar Vable and JaiHind Reddy Maddi. Boundary element analysis of adhesively bonded joints. *International Journal of Adhesion and Adhesive*, 26(3):133 – 144, 2006.

[13] M.R.B.Rodrigues R.Q.Rodriguez, P.Sollero. Analytical and numerical analysis of bonded joints and reinforcements by doublers in aeronautical structures. *21st Brazilian Congress of Mechanical Engineering*, 2011.

[14] M. Tekelioglu A. Kaya. Three dimensional stress analysis in adhesively bonded joints. *Department of Mechanical Education Sakarya University, Sakarya - Turkey*, 48(2):101–111, 1998.

[15] P. Lazzarin R. Afshar, F. Berto. Three-dimensional finite element analysis of single-lap joints: effect of adhesive thickness and poisson's ratio. *Key Engineering Materials*, 48(2):394–396, 2014.

[16] Petrolo M. Carrera E., Giunta G. Structures Classical and Advanced Beam Theories. 2008.

[17] A. Pagani E. Carrera, A.G. de Miguel. Hierarchical theories of structures based on legendre polynomial expansions with finite element applications. *International Journal of Mechanical Science*, pages 286–300, 2011.

[18] E. Zappino. *Variable kinematic 1D, 2D and 3D models for the Analysis of Aerospace Structures*. PhD thesis, Politecnico di Torino, 2014.

[19] M. Petrolo E. Carrera, A. Pagani. Use of Lagrange multipliers to combine 1D variable kinematic finite elements. *Elsevier Ltd*, 2013.

[20] E. Carrera and M. Petrolo. Refined beam elements with only displacement variables and plate/shell capabilities. *Meccanica*, 47(3):537–556, 2012.

[21] E. Carrera and M. Petrolo. Refined one-dimensional formulations for laminated structure analysis. *AIAA Journal*, 50(1):176–189, 2012.

[22] B. Szabó and I. Babuˇka. *Finite Element Spaces*, pages 145–165. John Wiley and Sons, Ltd, 2011.

[23] ASTM D35286. Standard test method for strength properties of double lap shear adhesive joints by tension loading. 2008.

[24] J.F. Durodola A. Beevers I. Pires, L. Quintino. Performance of bi-adhesive bonded aluminium lap joints. *International Journal of Adhesion & Adhesives*, pages 215–223, 2003.

[25] O. Oz H. Ozer. Three dimensional finite element analysis of bi-adhesively bonded double lap joint. *International Journal of Adhesion & Adhesives*, 48(2):50–55, 2012.